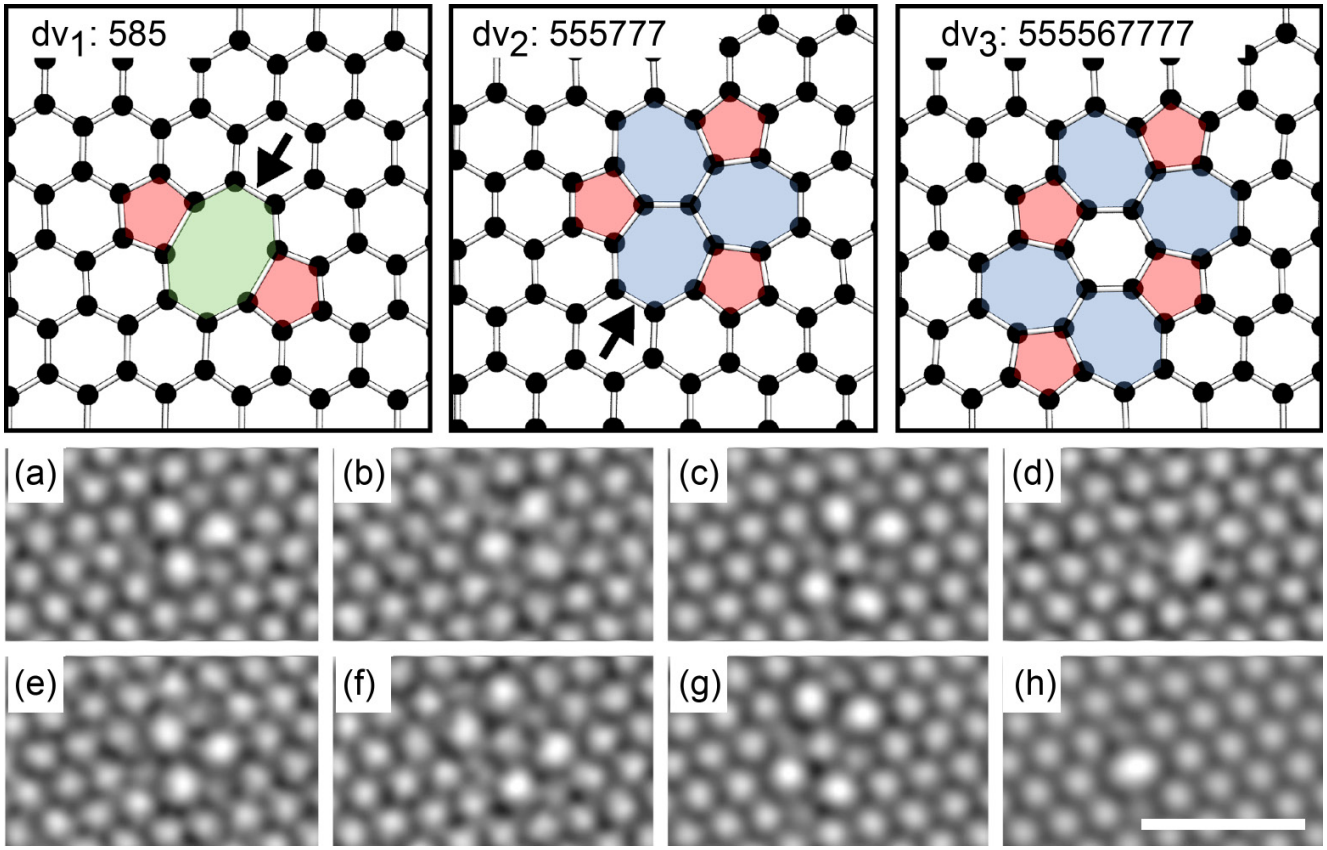

Figure 1. The three divacancy configurations in graphene and snapshots from an AC-HRTEM image sequence showing consequent transformations of the divacancy defect. The three top panels show ball-and-stick models of the divacancy defect in the three different structural states. Transformations between the states progress by rotating the bonds denoted by the arrows by 90°. (a – h) Subsequent states in which the same divacancy defect was observed. The scale bar corresponds to 1 nm.

Electron beam versus thermally driven transformations

Evidence against a universal electron-beam-induced virtual temperature exemplified for graphene

April 2016 - **Scientists from the Group of Electron Microscopy of Materials Science at Ulm University have attempted to measure the virtual temperature of single-layer graphene under the electron beam. They compared the relative population of three different divacancy defect states to the Boltzmann distribution using calculated energy levels of the defect states. They find that the measured populations cannot be fitted to the Boltzmann distribution, and consequently no universal virtual temperature can be assigned to the system.**

Coinciding breakthroughs in the electron optics for transmission electron microscopy (TEM) and in materials science have allowed rapid progression in the observation and understanding of atomic-scale processes in materials. First, the invention and practical realization of hardware spherical aberration correction (AC) in high-resolution TEM (HRTEM) and scanning TEM (STEM) pushed the resolution of the instruments to the atomic level even at lower acceleration voltages [1]. In these studies, the dynamics of 2D materials, such as graphene [2, 3], transition-metal dichalcogenides [4-6], 2D hexagonal boron nitride [7, 8], and 2D SiO_2 [9, 10], have been captured by aberration-corrected HRTEM and STEM.

The typical drivers of atomic-scale transformations are the thermal vibrations at an elevated temperature. In the Arrhenius-type description of the temperature dependence of reaction rates, local kinetic energies become occasionally high enough to overcome reaction barriers. Thus the reaction rate depends on the height of the reaction barrier and the sample temperature, which determines the average amplitude of the thermal fluctuations. In many cases the reaction barriers are so high that temperatures of thousands of degrees Kelvin are required for an observable reaction rate to manifest. Nevertheless, such high barrier reactions are readily observed in TEM, even if the sample is held at room temperature. For example, a bond rotation in graphene, where two atoms rotate 90° around their center point, has an estimated activation barrier of 5–10 eV [11]. For a reaction rate of 1/s to take place due to thermal vibrations, a temperature of roughly 2000–4000 K would be required.

It is widely accepted in the scientific community that the occurrence of transformations in graphene under the electron beam is induced by knock-on collisions [2]. That is, occasionally an energetic electron hits a target atom “head on“, leading to significant momentum transfer, which can push the system over the reaction barrier.

Furthermore, the electron beam can induce transformations in the target via excitations of the electronic systems. For many materials the total transformation rate can be a sum of both of the mechanisms [12]. During the transformation process, the sample is not significantly heated by the electron beam, meaning the processes are not activated by thermal vibrations. However, in earlier studies the transformations appeared to proceed as if the sample was held at an elevated temperature, and, indeed, the hypothesis of an electron-beam-induced "virtual temperature" has gained attraction in the scientific community.

To test this hypothesis, the scientists have investigated the case of divacancies in graphene, where three states are frequently observed (see the top panels in Fig. 1 for atomistic models, labeled dv_1, dv_2, and dv_3) [13]. The defect can transform from one state to the next one via bond rotations, where a pair of neighboring C atoms rotates 90° around their midpoint, and this process can be induced by the electron beam. Further examples of such transformations can be seen in the image sequence in Supplemental Movie 1 [14]. The dv_1 and dv_3 states can have three orientations in the hexagonal lattice, and the dv_2 two orientations, leading to degeneracies g_i of 3, 2, and 3 for the dv_1, dv_2, and dv_3 states, respectively. The formation energies, calculated by an analytical model of these structures are given in Table I.

State	$N_{i,t}$	$p_{i,t}$	E_f (eV)
dv_1	474	0.51 ± 0.04	7.7
dv_2	198	0.21 ± 0.03	6.8
dv_3	263	0.28 ± 0.03	7.1

TABLE I. The number of frames in which each divacancy state was detected, and the resulting probabilities, as in fractions of the total number of observations, and the calculated formation energies of each state.

To obtain the statistics, how often each of the defect states appears, the graphene sample was first explored until a divacancy defect was found. Point defects can be present in the pristine sample, or vacancies can be produced by the electron beam of the microscope [15]. Once a divacancy was found, an image sequence was recorded. Sequences of ten divacancies were recorded, adding up to 935 frames in total.

As results the dv_1 state is found to have the highest formation energy and the dv_2 the lowest (see Table I). As shown in the Supplemental Material [14], the use of the large simulation supercell is necessary to achieve fully converged energy values for the defects. In reality, the vacancies are never found in isolation, and indeed features such as contamination or other point defects can often be found within a few nanometers from the defects. To estimate the influence of interaction between point defects in close proximity, the scientists calculated the formation energies of pairs of divacancies in varying states and relative orientations and compared the energetics to the isolated cases. The results are summarized in the Supplemental Material of the publication [14]. The relevant conclusion from the calculations is that at distances of 3–4 nm the energy change is at maximum 0.1 eV and typically much less, meaning the energy hierarchy of the defect states does not change due to possible interaction with a neighboring defect. As a precaution, the authors limited the experimental analysis to cases where the distance to any nearby feature was at minimum 3.6 nm, and typically greater than that.

It becomes immediately clear that no meaningful fit of an exponential curve can be made to the data points (Fig. 2). In fact, the highest-energy state appears the most frequently, which would imply a negative temperature. 14% of the frames were discarded as unidentifiable, but even if one makes the extreme assumption that all of these frames represent the lowest-energy state dv_3, the high-energy dv_1 state would still remain the most common one. Consequently, the population of the defect states does not follow the Boltzmann distribution under the electron beam, and no virtual temperature can be defined for the system. Similar behavior of the self-interstitial dimer defect was, in fact, observed by the authors in an earlier experiment, where the lowest-energy configuration was observed the most seldom under the electron beam [3]. Furthermore, the electron energy loss plasmon spectrum of graphene does have peaks ranging from 4.7 to 14.5 eV [16], which are close to the range of expected energy barriers (5–10 eV [11]) for the transformations. The peak positions do not depend on the electron energy, which would be consistent with the close resemblance of the statistics gathered at 80 and 60 kV. All this would imply that the transformations of the divacancy defect would be driven through the electronic excitations.

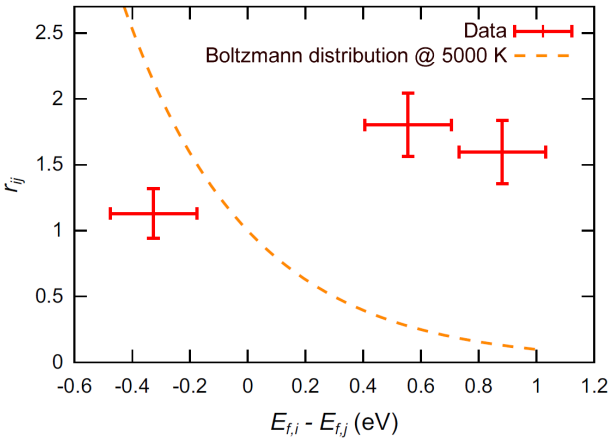

FIGURE 2. The relative probabilities of occupying the different divacancy states plotted against the energy differences of the states. An exponential function is plotted for reference.

For the system to precisely mimic high-temperature conditions, all of the undergoing processes should follow thermally activated behavior with no exceptions. Thus the universality of the high-temperature analogy breaks down with the counterexample presented in the new study. Taking into account the different nature of the excitations by thermal vibrations, and by impacts of energetic electrons, it is not an unexpected finding that the Boltzmann distribution is not followed by the population of the states under the electron beam. The results do not contradict the earlier findings, where in some cases the behavior of different structures under the electron beam has been similar to what could be expected at an elevated temperature. These need to be considered as special case, however, as the new experiment shows

that no meaningful universal virtual temperature can be determined for the excitement by the electron beam. Indeed, in all the prior experiments, attention has been directed to a specific subset of processes observed under the electron beam, and no attempt to describe the complete evolution of the sample has been made (this was not required for the aim of the studies either). With the new study, the scientists showed that great care needs to be taken when resorting to the analogy between electron beam and thermally driven transformations.

References

[†] Börner, P., Kaiser, U., & Lehtinen, O. (2016). Evidence against a universal electron-beam-induced virtual temperature in graphene. Physical Review B, 93(13), 134104, DOI: 10.1103/PhysRevB.93.134104

[1] Uhlemann, S., & Haider, M. (1998). Residual wave aberrations in the first spherical aberration corrected transmission electron microscope. Ultramicroscopy, 72(3), 109-119.

[2] Kotakoski, J., Meyer, J. C., Kurasch, S., Santos-Cottin, D., Kaiser, U., & Krasheninnikov, A. V. (2011). Stone-Wales-type transformations in carbon nanostructures driven by electron irradiation. Physical Review B, 83(24), 245420.

[3] Lehtinen, O., Kurasch, S., Krasheninnikov, A. V., & Kaiser, U. (2013). Atomic scale study of the life cycle of a dislocation in graphene from birth to annihilation. Nature communications, 4. (7 pages)

[4] Komsa, H. P., Kotakoski, J., Kurasch, S., Lehtinen, O., Kaiser, U., & Krasheninnikov, A. V. (2012). Two-dimensional transition metal dichalcogenides under electron irradiation: defect production and doping. Physical review letters, 109(3), 035503.

[5] Komsa, H. P., Kurasch, S., Lehtinen, O., Kaiser, U., & Krasheninnikov, A. V. (2013). From point to extended defects in two-dimensional MoS 2: evolution of atomic structure under electron irradiation. Physical Review B, 88(3), 035301.

[6] Lin, Y. C., Komsa, H. P., Yeh, C. H., Björkman, T., Liang, Z. Y., Ho, C. H., Huang, Y.-S., Chiu, P.-W, & Suenaga, K. (2015). Single-layer ReS2: Two-dimensional semiconductor with tunable in-plane anisotropy. ACS nano, 9(11), 11249-11257.

[7] Meyer, J. C., Chuvilin, A., Algara-Siller, G., Biskupek, J., & Kaiser, U. (2009). Selective sputtering and atomic resolution imaging of atomically thin boron nitride membranes. Nano letters, 9(7), 2683-2689.

[8] Cretu, O., Komsa, H. P., Lehtinen, O., Algara-Siller, G., Kaiser, U., Suenaga, K., & Krasheninnikov, A. V. (2014). Experimental observation of boron nitride chains. ACS nano, 8(12), 11950-11957.

[9] Huang, P. Y., Kurasch, S., Alden, J. S., Shekhawat, A., Alemi, A. A., McEuen, P. L., Sethna, J. P., Kaiser, U., & Muller, D. A. (2013). Imaging atomic rearrangements in two-dimensional silica glass: Watching silica's dance. Science, 342(6155), 224-227.

[10] Björkman, T., Kurasch, S., Lehtinen, O., Kotakoski, J., Yazyev, O. V., Srivastava, A., Smet, J., Kaiser, U., & Krasheninnikov, A. V. (2013). Defects in bilayer silica and graphene: common trends in diverse hexagonal two-dimensional systems. Scientific reports, 3.

[11] Li, L., Reich, S., & Robertson, J. (2005). Defect energies of graphite: density-functional calculations. Physical Review B, 72(18), 184109.

[12] Algara-Siller, G., Kurasch, S., Sedighi, M., Lehtinen, O., & Kaiser, U. (2013). The pristine atomic structure of MoS2 monolayer protected from electron radiation damage by graphene. Applied Physics Letters, 103(20), 203107.

[13] Banhart, F., Kotakoski, J., & Krasheninnikov, A. V. (2010). Structural defects in graphene. ACS nano, 5(1), 26-41.

[14] See Supplemental Material at http://link.aps.org/supplemental/10.1103/PhysRevB.93.134104 for AC-HRTEM image sequence showing transformations of the divacancy defect. Convergence of the formation energies with an increasing simulation system size: Interaction energies of adjacent divacancies.

[15] Meyer, J. C., Eder, F., Kurasch, S., Skakalova, V., Kotakoski, J., Park, H. J., Roth, S., Chuvilin, A., Eyhusen, S., Benner, G., Krasheninnikov, A. V., & Kaiser, U. (2012). Accurate measurement of electron beam induced displacement cross sections for single-layer graphene. Physical review letters, 108(19), 196102.

[16] Eberlein, T., Bangert, U., Nair, R. R., Jones, R., Gass, M., Bleloch, A. L., Novoselov, K. S., Geim, A., & Briddon, P. R. (2008). Plasmon spectroscopy of free-standing graphene films. Physical Review B, 77(23), 233406.